A model of the structure of HOO-Co•bleomycin bound to d(CCAG*T*ACTGG): recognition at the d(GpT) site and implications for double-stranded DNA cleavage

Dana E Vanderwall[1], Siu Man Lui[2], Wei Wu[2], Christopher J Turner[3], John W Kozarich[1] and JoAnne Stubbe[2]

Background: The bleomycins (BLMs) are a family of natural products used clinically as antitumor agents. In the presence of their required cofactors, iron and oxygen, BLMs bind to and mediate single-stranded and double-stranded DNA cleavage. Recently, two dimensional nuclear magnetic resonance (2D NMR) spectroscopic studies and molecular modeling have provided a picture of how the hydroperoxide form of cobalt BLM A2 (HOO-CoBLM), an analog of 'activated' iron BLM (HOO-FeBLM), binds to a d(GpC) motif and of the basis for both sequence specificity and chemical specificity of DNA cleavage.

Results: The solution structure of HOO-CoBLM bound to d(CCAG*T*ACTGG) containing a 'hot spot' for double-stranded DNA cleavage at *T*5 and *T*15 is reported using constraints from 2D NMR spectroscopy. The mode of binding and basis for sequence specificity and chemical specificity of cleavage is almost identical to that of a d(GpC) motif. This structure has allowed formulation of a structural model for how a single molecule of FeBLM can mediate a double-stranded DNA cleavage event without dissociation from the DNA.

Conclusions: The structural similarity of HOO-CoBLM bound to d(GpT) in d(CCAG*T*ACTGG) compared to a d(GpC) motif suggests a general paradigm for the binding of HOO-CoBLM to DNA and, by analogy, for the binding of the biological significant entity HOO-FeBLM.

Addresses: [1]Merck Research Laboratory, P.O. Box 2000, Rathway, NJ 07065-0900, USA. [2]Departments of Chemistry and Biology, Massachusetts Institute of Technology, Cambridge, MA 02139, USA. [3]Francis Bitter Magnet Laboratory, Massachusetts Institute of Technology, Cambridge, MA 02139, USA.

Correspondence: John W Kozarich and JoAnne Stubbe

Key words: bleomycin, DNA binding and recognition, double-stranded DNA cleavage, molecular modeling, NMR spectroscopy

Received: **26 March 1997**
Accepted: **24 April 1997**

Chemistry & Biology May 1997, **4**:373–387
http://biomednet.com/elecref/1074552100400373

Introduction

The bleomycins (BLMs; Figure 1) are natural products isolated from *Streptomyces verticillus* that are used clinically in the treatment of head, neck, and testicular cancers and squamous cell carcinomas [1–3]. They have been the focus of intensive studies since their discovery and the mechanism of their cytotoxicity is thought to be related to their ability to bind to double-stranded (ds) DNA and in the presence of ferrous iron, oxygen and a reductant, to catalyze DNA strand scission [4–6]. Both single-stranded (ss) and ds cleavage events occur with single-stranded predominating [7]. The ds breaks, which are thought to be more difficult to repair, have been proposed to be the source of BLM's cytotoxicity [7]. Recent studies have also shown that metallo-BLMs can bind to and cleave RNA–DNA hybrids as well as to unusual RNA structures [8–10]. The relationship of these studies to clinical cytotoxicity remains to be established.

Studies in the past two decades [11,12] have revealed the chemistry of the reductive activation of oxygen by FeBLM in which an iron hydroperoxide (HOO-FeBLM, designated activated BLM) is generated. This is the last detectable iron species in the cleavage process [13]. Studies have also revealed the details of the chemistry at the C4′ position of the deoxyribose of the pyrimidine (Py) in the d(GpPy) motif, the site of the initiation of ss and ds cleavage events [5,14]. Although the molecular mechanism of ss cleavage of DNA by BLMs is relatively well understood [5,14–18], an understanding of the ds cleavage process has only recently begun to emerge [19–23]. These studies have been interpreted to support a model in which a single molecule of BLM can catalyze cleavage on both strands without dissociating from DNA. The structural basis for this proposal and the sequence and chemical specificity of ss and ds cleavage events have recently been the focus of many laboratories [23–31].

Our laboratories [23,26–28] and that of Petering and coworkers [24] have chosen to investigate the interaction of the hydroperoxide form of cobalt BLM A2 (HOO-CoBLM or CoBLM A2 green), which we have proposed might be an excellent analog of activated iron BLM (HOO-FeBLM), with a deoxyoligonucleotide containing a single binding and cleavage site. Our two-dimensional nuclear magnetic resonance (2D NMR) studies of HOO-CoBLM with d(CCAGG*C*CTGG) (1) — *C* is the site of cleavage — in conjunction with molecular modeling studies have

Figure 1

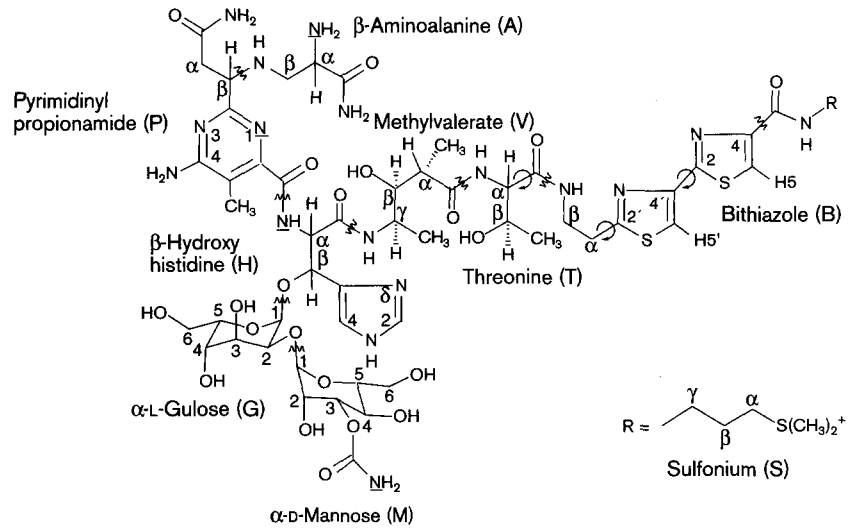

Structure of bleomycin A2. The arrows indicate the bonds about which rotations have been made in the modeling studies of the doubled-stranded DNA cleavage process (see the Results and discussion section). The junctions between the molecular units comprising bleomycin A2 are indicated by wavy lines. The underlined N atoms are the putative ligands to the metal required for cleavage.

identified the importance of the 4-amino group and N3 of the pyrimidine of HOO-CoBLM in defining the basis of the specificity for guanine 5′ to the cleavage site [28]. This work has also established that the bithiazole tail is responsible for binding to DNA by partial intercalation 3′ to the cleavage site. This model has further revealed a basis for 4′ chemistry at the cytidine in the dGpC motif [28]. Mao *et al.* [24] have recently reported their preliminary studies examining the interaction of HOO-CoBLM with two additional sequences: d(GGAAG*C*TTCC) and d(AAACG*T*TT). Although no model was presented in these studies, examination of reported chemical shift and nuclear Overhauser enhancement (NOE) data suggests a similar mode of binding and basis for sequence specificity to those we obtained with **1**. To determine whether our model for dGpC motifs is representative of HOO-CoBLM's interaction with d(GpT) motifs, we have investigated its interaction with d(CCAG*T*ACTGG) (**2**). This oligonucleotide has the added appeal that G*T*AC is a 'hot spot' for ds cleavage [21,22]. A model of the HOO-CoBLM•2 complex, which has been determined by 2D NMR analysis in conjunction with molecular modeling, is reported. These studies have established the similarities in the recognition of HOO-CoBLM for dGpC and dGpT motifs and provided insight into how a single molecule of BLM could be involved in the ds cleavage process.

Results and discussion

Recent studies of Absalon *et al.* [21,22] revealed that GTAC is a hot spot for ds cleavage (at T) with a ratio of ss:ds cleavage events of 3:1. Thus, in order to determine if HOO-CoBLM interacts with dGpT motifs, in an analogous fashion to its previously reported interactions with dGpC motifs and in an effort to gain insight into the structural basis of the ds cleavage process, we have used 2D NMR methods and molecular modeling to investigate the structure of HOO-CoBLM with **2**.

As previously described in detail [23,27,28] the choice of HOO-CoBLM was dictated by our hypothesis that it is an excellent mimic of the activated iron BLM (HOO-FeBLM). Although the chemistry of DNA cleavage differs between the Co(III) and Fe(III) analogs, the sequence specificity of cleavage at Py in dGpPy sequences, and the chemical specificity of cleavage at 4′ hydrogen are very similar [32–34].

Our preliminary studies showed that HOO-CoBLM binds to **2** with an apparent K_d of 1.5×10^{-7} M, and is capable of light-mediated ss cleavage, uniquely at T5 [27]; ds cleavage has not been observed with the cobalt analog, which is not surprising considering the difference in the detailed chemistry relative to iron.

The 1D titration of HOO-CoBLM with **2** revealed that it forms a mixture of two complexes in a ratio of 4:1, both in slow exchange with the free DNA on the NMR time scale [27]. To date, our efforts have focused on obtaining a model structure of the major complex.

Assignments of nonexchangeable protons of DNA

Assignment of the protons of **2** when it was complexed with HOO–CoBLM was carried out by analyzing the spectra of double quantum filtered correlation spectroscopy (DQF-COSY), total correlation spectroscopy (TOCSY), NOE spectroscopy (NOESY), and ^{31}P–^{1}H COSY experiments in

Table 1

The assignments of ^{1}H chemical shifts of 2 bound to HOO-CoBLM in 50 mM NaPi (pH 6.8) at 20°C.

	H6/H8	H5/H2	H1′	H2′	H2″	H3′	H4′	H5′/5″	Methyl	^{31}P
C1	7.76	5.90	5.91	2.26	2.58	4.65	4.08	3.76/3.76		−0.30
C2	7.71	5.76	5.75	2.24	2.51	4.88	4.64	4.08/4.08		−0.32
A3	8.11	7.59	6.21	2.63	3.00	5.06	4.46	4.05/4.20		−0.81
G4	7.80		5.54	2.66	2.31	5.02	4.49	4.30/4.29		1.10
T5	7.14		5.84	1.86	2.18	4.81	3.24	4.01/3.84	1.45	−0.12
A6	8.34	7.56	6.04	2.70	2.74	4.88	4.17	3.32/3.81		−0.74
C7	7.37	5.18	5.95	1.97	2.41	4.72	4.27	4.14/4.14		−0.20
T8	7.29		5.60	1.96	2.24	4.81	4.26	4.09/4.09	1.57	0.12
G9	7.82		5.62	2.66	2.70	4.97	4.34	3.98/4.07		−0.09
G10	7.79		6.10	2.33	2.52	4.97	4.64	4.09/4.18		
C11	7.69	5.86	5.89	1.99	2.44	4.62	4.07	3.70/3.70		−0.29
C12	7.56	5.66	5.23	2.13	2.35	4.83	4.62	4.08/3.99		−1.30
A13	8.18	7.68	6.03	2.77	2.88	5.03	4.39	4.11/3.99		−0.80
G14	7.54		5.75	2.36	2.55	4.90	4.31	4.19/4.09		−0.16
T15	6.94		5.88	2.09	2.36	4.83	4.90	4.12/4.20	1.19	0.85
A16	8.13	7.24	6.12	2.61	2.93	4.87	4.38	4.13/4.12		−0.27
C17	7.20	5.28	5.30	2.03	2.20	4.40	4.29	4.11/4.23		−0.70
T18	7.34		5.91	1.98	2.57	4.79	3.70	3.93/3.93	1.55	−1.26
G19	7.65		5.25	2.37	2.47	4.80	4.20	3.97/3.73		0.15
G20	7.72		6.11	2.33	2.38	4.58	4.20	4.06/4.06		

	Imino	Cytosine amino
C1•G20		
C2•G19	12.99	8.57/6.87
A3•T18	12.91	
G4•C17	12.84	8.25/6.73
T5•A16	13.25	
A6•T15	13.30	
C7•G14	12.51	7.87/6.50
T8•A13	14.09	
G9•C12	12.91	8.62/6.06
G10•C11		

D_2O and/or H_2O using standard sequential strategies [35]. Proton assignments are summarized in Table 1.

Our previous NMR studies of HOO-CoBLM bound to **1** revealed that the bithiazole tail binds via partial intercalation, inserting itself from the minor groove, 3′ to the cleavage site [26,28]. Analysis of the expanded NOESY spectrum in the base to H1′ region (Figure 2) of strand 1 (C1–G10) revealed a break in the intrastrand sequential connectivities between A6–H8 and T5–H1′. There was also disruption in the second strand (C11–G20) between A16–H8 and T15–H1′ (data not shown). These results are consistent with an intercalative mode of binding 3′ to the T5 cleavage site.

Assignments of exchangeable protons of DNA

Assignment of the sequential imino protons also provides an easy method to evaluate an intercalative mode of binding [28]. In the case of **2**, this task was more difficult than for **1**. All the imino protons are observed between 12.5 ppm and 13.3 ppm from both the major and minor complexes leading to spectral overlap. Despite this problem, the use of intramolecular NOEs between the G•C imino proton and H5 of its cytosine, the A•T imino proton and the H2 of its adenine and the CH_3 of its thymine, has confirmed the assignments (Table 1). The presence or absence of an NOE between the imino protons of T5•A16 and A6•T15 is obscured due to overlap with the diagonal peaks.

Unexpectedly, the chemical shift of the A3•T18 imino proton was shifted upfield from 14.02 ppm in free DNA to 12.91 ppm in the complex and contrary to expectations based on observations with other intercalators [36,37] and HOO-CoBLM complexed with **1** [28], the imino protons associated with T5•A16 (13.25 ppm) and A6•T15 (13.30 ppm) were not shifted upfield relative to free DNA (13.37 ppm, Table 1 and Table 2). We will return to these points after the discussion of our model structure.

Assignments of ^{31}P resonances of DNA

^{31}P NMR has frequently been used as a probe to monitor conformational changes associated with an intercalative mode of binding as well as to confirm certain ^{1}H chemical shift assignments [36–38]. Nine phosphorus resonances are observed in free **2**, that are doubled on complexation

Figure 2

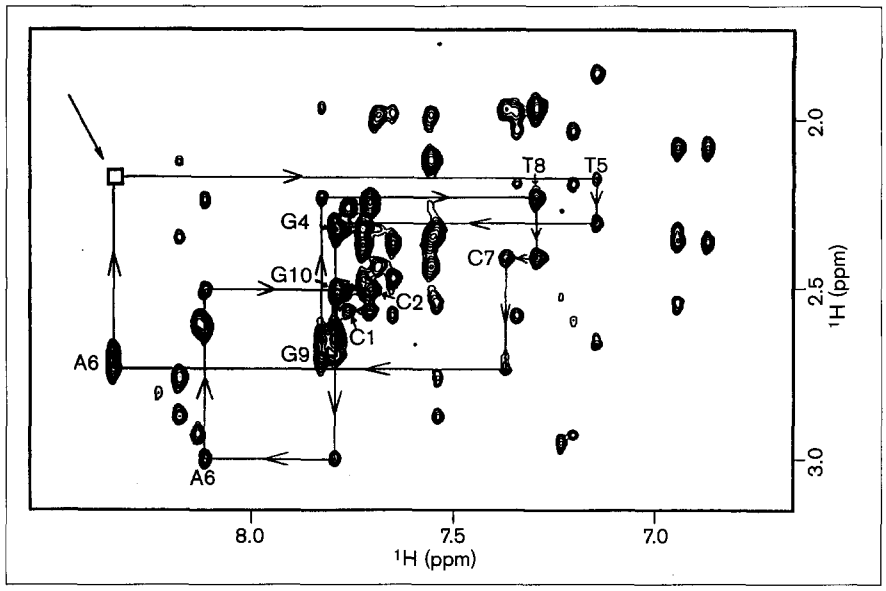

Expanded NOESY spectrum of the complex (D_2O, 400 ms mixing time, 750 MHz) of the base to sugar H1′ of strand 1 (C1–C2–A3–G4–T5–A6–C7–T8–G9–G10). The sequential connectivities are indicated by the connecting lines, and the break is shown by an empty box (upper left arrow) at T5–A6.

with HOO-CoBLM. Two of the phosphorus signals are downfield shifted 1–1.5 ppm from free DNA and have been assigned to the G4pT5 and T15pA16 phosphates by ^{31}P–^{1}H COSY experiments (Figure 3, Table 1). Similar chemical shift changes were observed at the corresponding phosphates in **1**, although the magnitude of the shifts (1.5–2 ppm) was larger [28].

Assignments of protons in the HOO-CoBLM complexed with 2

The use of DQF-COSY, TOCSY, and NOESY spectra of HOO-CoBLM bound to **2** in D_2O and/or H_2O have allowed assignments of the chemical shifts of all of its protons with the exception of those associated with the gulose and mannose moieties (Figure 1) [27,28,39–41]. The strategies used for these assignments are analogous to those previously described in detail [28], and the results are summarized in Table 3. The chemical shifts of HOO-CoBLM complexed with **2** are very similar to those previously reported with **1** and only the protons with unusual chemical shifts will be highlighted.

The assignments of the protons associated with the bithiazole moiety (B in Figure 1) are essential for defining its mode of binding to DNA. Previous studies by Akkerman *et al.* [40,41] used ^{13}C–^{1}H heteronuclear multiple-quantum

Table 2

The assignments of ^{1}H chemical shifts of free 2 in 50 mM NaPi (pH 6.8) at 20°C.

	H6/H8	H5/H2	H1′	H2′	H2″	H3′	H4′	Methyl
C1	7.74	5.95	5.97	2.04	2.49	4.66	4.11	
C2	7.57	5.70	5.35	2.10	2.38	4.84	4.10	
A3	8.24	7.70	6.08	2.83	2.93	5.07	4.40	
G4	7.63		5.85	2.48	2.71	4.90	4.19	
T5	7.17		5.73	2.05	2.05	4.86	4.18	1.38
A6	8.26	7.36	6.20	2.69	2.86	5.01	4.43	
C7	7.30	5.20	5.82	1.90	2.87	4.71	4.19	
T8	7.28		5.63	1.92	2.34	4.82	4.08	1.59
G9	7.84		5.65	2.67	2.67	4.97	4.38	
G10	7.82		6.15	2.35	2.53	4.65	4.21	
		Imino				Cytosine amino		
C1•G20								
C2•G19		13.00				8.60/6.89		
A3•T18		14.02						
G4•C17		12.70				8.00/6.61		
T5•A16		13.37						

Figure 3

^{31}P–^{1}H COSY spectrum of the complex at 30°C (600 MHz for ^{1}H). Note the unusual upfield chemical shift of the H4′ proton of T5 at the site of cleavage.

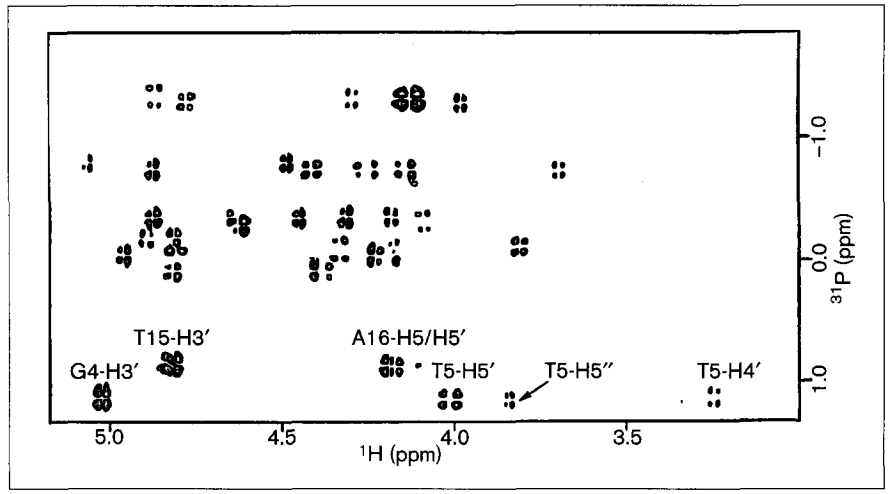

coherence (HMQC) spectroscopy and heteronuclear multiple bond correlation (HMBC) spectroscopy, to assign the B–H5 and B–H5′ protons. We have previously used this strategy [27,28], as have Xu *et al.* [39], to assign these protons in HOO-CoBLM. The HMQC method applied to the complex with **2**, assuming that the ^{13}C chemical shift of the carbons attached to each of these protons is not very different in the complex relative to free HOO-CoBLM, has allowed the assignment of B–H5 to a resonance at 6.87 ppm and B–H5′ to one at 7.04 ppm. These protons are shifted upfield by 1.30 ppm and 0.78 ppm relative to free HOO-CoBLM (Table 3). These upfield shifts are similar to those observed previously with **1** and support an intercalative mode of binding with **2**. Further support for this

Table 3

^{1}H and ^{13}C chemical shifts (ppm) of free and bound HOO-CoBLM in 50 mM NaPi (pH 6.8) at 20°C.

		^{13}C		^{1}H	
		Free	Bound	Free	Bound
P	CαH	35.5		3.20	2.78
	CαH′	35.5		3.51	3.65
	CβH	65.1	65.5	5.10	5.04
	CH_3	12.0	12.3	2.46	2.67
	4-NH_2			7.73,7.94	7.07,10.23
H	CαH	60.1	61.0	4.98	5.03
	CβH	71.7	72.4	5.53	5.50
	C2H	144.8	147.2	8.72	9.18
	C4H	122.2	121.5	7.60	7.60
A	CαH	59.3	60.5	3.41	3.37
	CβH	51.8	50.0	2.74	2.41
	CβH′	51.8	50.0	3.22	3.39
	NH			6.01	5.80
V	αCH_3	9.81	9.48	0.62	0.67
	γCH_3	20.4	20.4	0.98	0.96
	CαH	42.9	41.4	0.94	1.22
	CβH	77.7	75.8	3.33	3.74
	CγH	49.6	50.1	3.50	3.50
	NH			8.89	8.76
	OH				6.75
T	CH_3	22.4	21.8	1.19	1.26
	CαH	60.0	59.0	4.39	4.55
	CβH	71.7	73.3	4.25	4.55
	NH			8.92	9.39
B	CαH	35.5	40.5	3.06	2.28
	CαH′	35.5	40.5	3.25	2.52
	CβH	41.9	43.6	3.44	2.96
	CβH′	41.9	43.6	3.83	3.75
	C5H	127.5	125.3	8.17	6.87
	C5′H	121.3	118.0	7.82	7.04
	NH			8.57	8.64
S	C$αH_2$	43.4	43.2	3.36	3.40,3.62
	C$βH_2$	26.6	26.0	2.13	2.14,2.23
	CγH	40.3	40.1	3.51	3.44
	CγH′	40.3	40.1	3.63	3.50
	$(CH_3)_2$	27.3	27.4	2.94	2.97
	NH			8.66	8.39
G	C1H	97.4	98.7	5.35	5.44
	C2H	69.9	70.4	4.11	4.09
	C3H	68.4	68.0	4.10	4.18
	C4H	71.8		3.80	3.78
	C5H	70.8		3.84	3.92
	C6H	63.9		3.70	
	C6H′	63.9		3.84	
M	C1H	98.5	102.0	4.93	5.02
	C2H	70.3		4.00	3.96
	C3H	77.6		4.05	
	C4H	66.7		3.78	
	C5H	77.0		3.73	
	C6H	63.5		3.84	
	C6H′	63.5		3.98	
CoOOH					8.84

model is provided by NOEs observed between B–H5′ and protons associated with T5 and T15, and between B–H5 and protons associated with T15 and A16 (Table 4).

Our previous studies [28] with **1** further identified two exchangeable protons associated with HOO-CoBLM that proved to be quite informative: one at 10.36 ppm and one at 8.89 ppm. The former was shown to be associated with one of the 4-amino protons of the pyrimidine of BLM, and shown by modeling to be involved in sequence specificity for guanine, 5′ to the cleavage site. The corresponding observation of an exchangeable proton at 10.23 ppm in the complex with **2** is intriguing. This proton exhibits a strong NOE to another exchangeable proton at 7.07 ppm, presumably the second proton of the 4-amino group of the pyrimidine of BLM. Both these protons (P-NH_2) show medium intensity NOEs to the P-CH_3 (Table 5) and exhibit NOEs to H4′, H2″, and H1′ of G4 and H2 of A3 (Table 4). The observed large downfield shift of one of the 4-amino protons relative to the protons at 7.73 ppm and 7.94 ppm of free HOO-CoBLM and the observed NOEs to DNA in the minor groove suggest that this proton interacts with DNA by hydrogen bonding in a manner analogous to that previously observed in the complex of HOO-CoBLM with **1** [28].

A second exchangeable proton, observed at 8.84 ppm, was previously observed at 8.89 ppm in the complex with **1** [28]. This proton shows four intermolecular NOEs to T5 (H4′, H2′, H2″ and H1′; Table 4) and ten intramolecular NOEs to the protons associated with HOO-CoBLM (H-C2H, P-CβH, V-αCH_3, V-γCH_3, V-CαH, V-NH, T-CαH, T-CβH, T-NH, and B-CβH) (Table 5). There is no detectable through-bond coupling between this proton and any other proton in either TOCSY or DQF-COSY spectra. Although several exchangeable protons remain unassigned in the complex, it is unlikely that this proton is associated with DNA itself because there is no NOE observed between it and any of the imino or amino protons of the DNA. The ample number of intermolecular NOEs to the minor groove protons at the T5 cleavage site and the intramolecular NOEs to the protons in the linker region, in conjunction with modeling studies (described subsequently) support the assignment of this proton to that associated with the hydroperoxide ligand. The ability to detect this proton may be attributed to its seclusion from the solvent and the putative hydrogen bonding interaction with the carbonyl of the T moiety of BLM, as revealed through the molecular modeling discussed later.

Finally, the perturbations of chemical shifts of a number of protons associated with HOO-CoBLM relative to free HOO-CoBLM and intermolecular NOEs with protons in the minor groove of DNA in the vicinity of the cleavage site, further support the minor-groove binding of the metal-binding domain adjacent to the site of cleavage. The

Table 4

The intermolecular NOEs between HOO-CoBLM and 2 in 50 mM NaPi (pH 6.8) at 20°C.

5′ end	Strand 1	BLM residues	Intensity of NOE‡	BLM residues	Intensity of NOE	Strand 2	3′ end
A3	H2	P-NH_2(1)†	m	A-CαH	w	H5′*	T18
		P-NH_2(2)†	m	A-CβH	w		
				A-CβH′	w		
				A-CαH	m	H4′	
				A-CβH	m		
				A-CβH′	m		
				A-CβH′	m	H1′	
G4	H5′*	P-CH_3	m				C17
	H4′	P-CH_3	s				
		P-NH_2(1)†	m				
		P-NH_2(2)†	w				
	H2″	P-NH_2(1)†	w				
	H1′	P-CH_3	m				
		P-NH_2(1)†	s				
		P-NH_2(2)†	w				
	NH	P-CαH′	w				
T5	H5′	P-CH_3	s	B-CαH	w	H2	A16
		V-γCH_3	m	B-CαH′	w		
	H5″	P-CH_3	s	B-CβH	m		
		V-γCH_3	m	B-CβH′	m		
	H4′	P-CH_3	m	P-CαH′	w		
		V-γCH_3	s	B-C5H	m	H8	
		Co-OOH	m				
		V-NH	w				
	H3′	V-γCH_3	w				
	H2″	V-γCH_3	w				
		B-CβH′	w				
		Co-OOH	m				
	H2′	B-CβH′	w				
		V-γCH_3	w				
		Co-OOH	w				
	H1′	P-CH_3	w				
		P-CβH	w				
		Co-OOH	m				
		B-CβH′	m				
	CH_3	B-C5H′	m				
		S-$(CH_3)_2$	w				
	NH	B-C5H′	m				
A6	H4′	B-NH	m	B-C5H	m	H5′*	T15
		T-Cα/βH	w	B-C5H	m	H3′	
		T-CH_3	m	B-C5H	m	H2′	
	H5′*	T-Cα/βH	m	B-C5H	m	H2′	
		V-γCH_3	w	B-C5H	w	H1′	
	H1′	B-NH	w	B-C5H	m	CH_3	
				B-C5H′	w		
				S-CγH	s		
				S-CγH′	m		
				S-CβH	m		
				B-C5H′	w	NH	

*Denotes the cases where pseudoatoms are used. †P-NH_2(1) and P-NH_2(2) are the hydrogens at 10.23 ppm and 7.07 ppm, respectively. ‡w, m and s denote weak, medium and strong NOEs, respectively, observed in a NOESY spectrum (200 ms mixing time).

Table 5

The nontrivial intramolecular NOEs* within HOO-CoBLM complexed with 1 and 2 at 20°C.

NOE	1	2	NOE	1	2	NOE	1	2
H-C2H···A-CβH	w		A-CβH′···P-CαH′	w	m	T-NH···T-CH_3		w
H-C2H···A-CβH′	w		A-CβH···P-CβH	w	w	T-NH···V-CβH		m
H-C2H···A-NH	m	m	A-CβH′···P-CβH	w	w	T-NH···T-CαH		w
H-C2H···P-CβH	w	w	A-CαH···P-CαH	w		T-NH···T-CβH		w
H-C2H···T-CH_3	m	s	A-CαH···P-CβH		w	B-NH···T-CH_3	m	m
H-C2H···T-CβH	w	m	A-CβH···P-CαH	m	m	B-NH···B-CαH	m	w
H-C2H···T-CαH	w	m	A-CβH′···P-CαH	m	m	B-NH···B-CαH′	m	w
H-C2H···T-NH	w	m	V-γCH_3···P-CH_3	w	m	B-NH···B-CβH		m
H-C2H···V-CαH	m	m	V-γCH_3···V-CβH	s	s	B-NH···B-CβH′		m
H-C2H···V-αCH_3	w	m	V-γCH_3···V-CαH	m	m	B-C5′H···S-NH		w
H-C2H···V-CβH	w	w	V-αCH_3···V-CγH	s	s	B-C5H···S-NH		w
H-C4H···V-CαH	w	m	V-αCH_3···H-CβH	w	w	B-C5H···S-CγH		w
H-C4H···V-αCH_3	m	s	V-αCH_3···V-CβH	m	s	S-CαH···S-CH_3	w	w
H-C4H···H-CαH	w	m	V-αCH_3···V-γCH_3	m	m	S-CαH′···S-CH_3	w	w
H-C4H···H-CβH		s	V-CαH···V-CβH		s	G-C1H···M-C1H	m	m
H-C4H···G-C1H		m	V-CαH···V-CγH		s	M-C1H···H-CβH	w	
H-CαH···V-γCH_3		w	V-NH···V-γCH_3	s	m	Co-OOH···H-C2H		w
H-CαH···G-C1H	m	m	V-NH···V-αCH_3	s	m	Co-OOH···V-αCH_3	w	w
H-CβH···V-γCH_3		w	V-NH···V-CαH	s	m	Co-OOH···V-γCH_3	w	w
H-CβH···V-CγH	w	w	V-OH···V-αCH_3	w	w	Co-OOH···V-CαH	m	w
H-CβH···G-C1H	s	s	V-OH···V-γCH_3	s	m	Co-OOH···T-CαH	m	w
P-CβH···B-CβH′	w	w	V-OH···V-CβH	s	m	Co-OOH···T-CβH	m	w
P-CβH···P-CαH′		m	T-NH···V-CαH	m	m	Co-OOH···P-CβH		m
P-CβH···P-CαH		m	T-NH···V-NH	m	w	Co-OOH···B-CβH		m
P-NH2 (1)···P-CH_3	m	m	T-NH···V-αCH_3		m	Co-OOH···T-NH	m	m
P-NH2 (2)···P-CH_3	m	m	T-NH···V-γCH_3		w	Co-OOH···V-NH	w	w
A-NH···T-CH_3	w	w				Co-OOH···V-CγH	w	
A-CβH···P-CαH′	m	w						

*w, m, and s denote weak, medium, and strong NOEs, respectively, observed in a NOESY spectrum (200 ms mixing time).

chemical shift perturbations of >0.4 ppm are detected for P-CαH, B-CαH, B-CαH′, B-CβH, T-NH, V-CbH, and H-C2H (Figure 1, Table 3). The methyl groups of the P and V moieties exhibit intermolecular NOEs to H4′ and H1′ of G4, and H5′, H5″, H4′, and H1′ of T5, respectively. Support for the primary amine of the β-aminoalanine moiety as an axial ligand to cobalt in the complex is also apparent. Although the assignments of the β-aminoalanine spin system were difficult, methods identical to those used previously for HOO-CoBLM with **1** proved to be successful [28]. Furthermore, the small coupling constant (<4 Hz) associated with the A-CαH and A-CβHs, suggest that the conformation of this ligand is similar to that in the complex with **1**. The assignment of A-CαH and CβHs allowed the detection of NOEs to the H5″, H5′, H4′, and H1′ of T18, further supporting the assignment of the primary amine of β-aminoalanine moiety as an axial ligand and suggesting a similar orientation of the metal-binding domain relative to the site of cleavage. Observation of NOEs between H-C2H and protons associated with the T and V moieties (Table 5), similar to those observed with free HOO-CoBLM [27], suggest a folded conformation in the complex similar to that observed in solution. Finally, no NOEs were detected between the DNA and the assigned protons of the gulose and mannose residues indicating there are no specific interactions associated with the sugar domain.

Molecular modeling

The substantial number of intermolecular NOEs observed between the protons associated with the bithiazole tail and the minor-groove protons associated with DNA (Table 4) assisted in the initial docking of HOO-CoBLM to DNA. Specifically, the B moiety was positioned between base pairs T5•A16 and A6•T15. This initial structure was then minimized and molecular dynamics simulated annealing calculations (see the Materials and methods section) were performed as described previously [28]. 20 separate calculations were carried out, 18 of which exhibited low experimental constraints violations. A final structure was generated by averaging these 18 structures and then minimizing the averaged structure. An overlay of these 18 structures is shown in Figure 4a and a summary of the structural statistics is shown in Table 6. Geometries and statistics described below are the mean value of the 18 structures ± standard deviation. It should be emphasized that the 18 structures were generated from the molecular modeling described in the Materials and methods section. Thus, the accuracy and precision of the distances, angles, and their standard deviations reported herein are necessarily affected by errors associated with assigning NOE sizes, the uneven distribution of distance constraints and limitations of the molecular dynamics protocol itself.

Figure 4

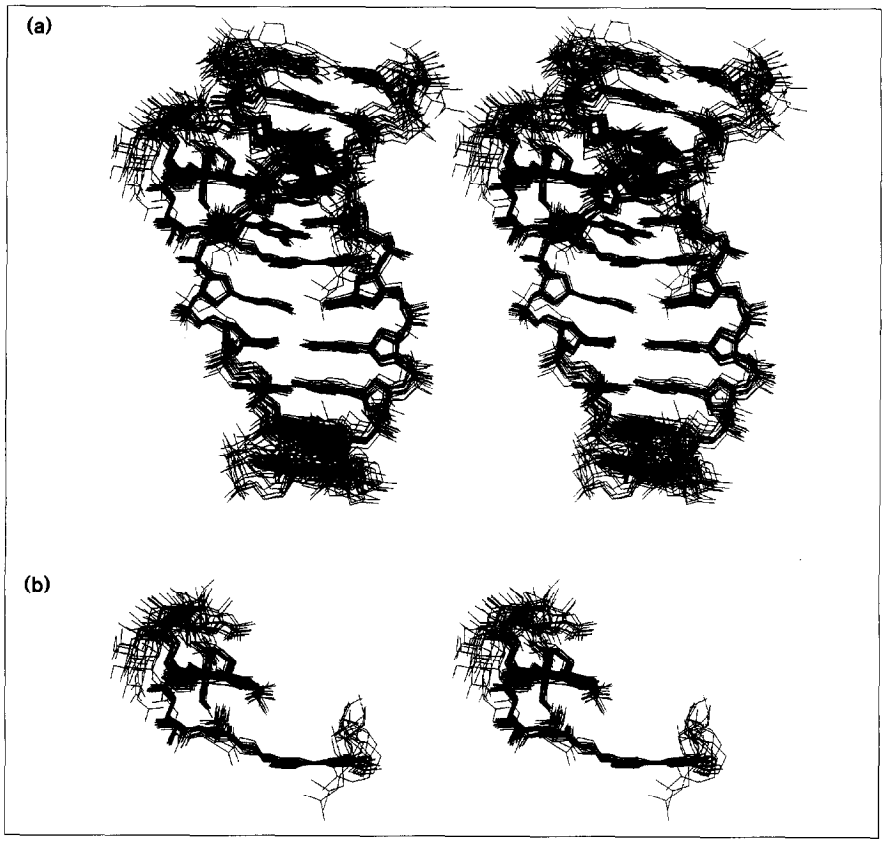

A stereo view of the 18 calculated structures of HOO-CoBLM bound to **2**. **(a)** The complex of HOO-CoBLM with **2** from a view in which the strand containing the T5 cleavage site is in the foreground running 5′→3′ from the top right of the figure to the bottom left side. **(b)** The HOO-CoBLM from the complex with **2**, viewed in the same orientation as the complex shown in (a).

Overall structure

The final structural model of HOO-CoBLM complexed with **2** is shown in Figure 5. Its mode of binding and basis for sequence specificity in this d(GpT) motif is remarkably similar to that previously observed in the complex with **1** (dGpC) [28]. The bithiazole tail binds by partial intercalation between base pairs T5•A16 and A6•T15, and the positively charged sulfonium tail extends into the major groove. The linker region (V and T moieties) is positioned in the minor groove, 3′ to the cleavage site T5. The backbone of the V and most of the T moieties adopt a conformation very similar to that observed free in solution and in the complex with **1** [27,28]. The N3 and 4-amino groups of pyrimidine are within hydrogen bonding distance to the 2-amino group and the N3 of G4, respectively, 5′ to the cleavage site. As a result of these specific interactions and the intercalative mode of binding, the terminal oxygen of the axial hydroperoxide ligand of the cobalt is positioned 2.4 ± 0.2 Å from the 4′-hydrogen of T5. This model structure suggests that, although subtle differences (to be discussed below) exist, the recognition for the dGpT motif is very similar to that previously established for a dGpC motif [28].

Table 6

Structural statistics for the complex of HOO-CoBLM with 2.

Total number of distance constraints	383
HOO-CoBLM···DNA intermolecular	59
HOO-CoBLM intramolecular	75
DNA intramolecular	223
DNA base pair hydrogen bond	26
Rms deviation from experimental distance constraints in the final 18 structures (Å)	0.026 ± 0.002
Maximum error (Å)	0.21 ± 0.02
Σ Distance constraint errors (Å)	3.6 ± 0.3
Rms deviation from dihedral angle constraints in the final 18 structures (degrees)	6 ± 3
Pairwise rms deviation of the final 18 structures from the average structure (Å) for:	
All atoms	1.17 ± 0.23
'Core structure' (non-hydrogen atoms, excluding DNA ends and S, G, and M moieties of HOO-CoBLM*)	0.53 ± 0.12
HOO-CoBLM, excluding S, G, and M	0.32 ± 0.13

*DNA nucleotides 3–8, 13–18, and the bound HOO-CoBLM without the G, M, and S moieties.

Mode of binding and basis for sequence specificity

The intermolecular NOEs between the protons of 2 and the B and S moieties of HOO-CoBLM (Figure 1; Table 4) clearly define the position of the bithiazole tail between the T5•A16 and A6•T15 base pairs, as well as the *trans*

Figure 5

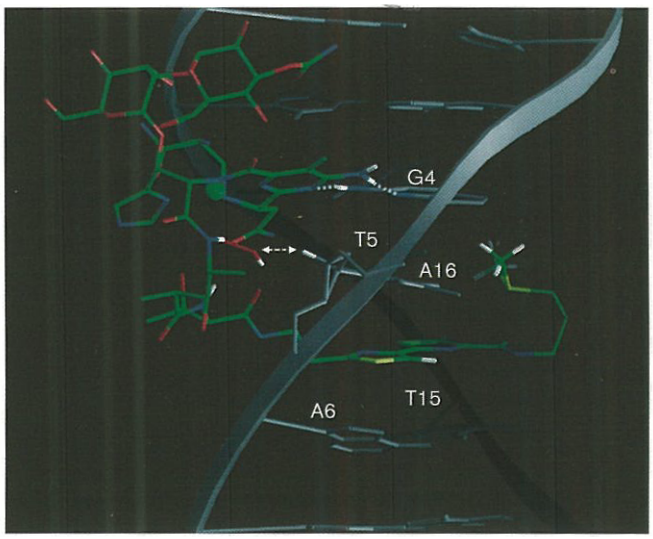

The final averaged structure of HOO-CoBLM bound to DNA. Atoms of HOO-CoBLM are coloured by element: C, green; O, red; N, blue; S, yellow; DNA, gray; T5–H4′, white. The strand on which the first cleavage occurs is in the foreground, running 5′→3′ from the upper right to lower left corner. The dotted lines indicate the modeled hydrogen-bond interactions between the pyrimidine moiety (P in Figure 1) of the HOO-CoBLM and G4 of DNA. The arrow indicates the proximity of the distal oxygen of the hydroperoxide ligand to T5–H4′.

Figure 6

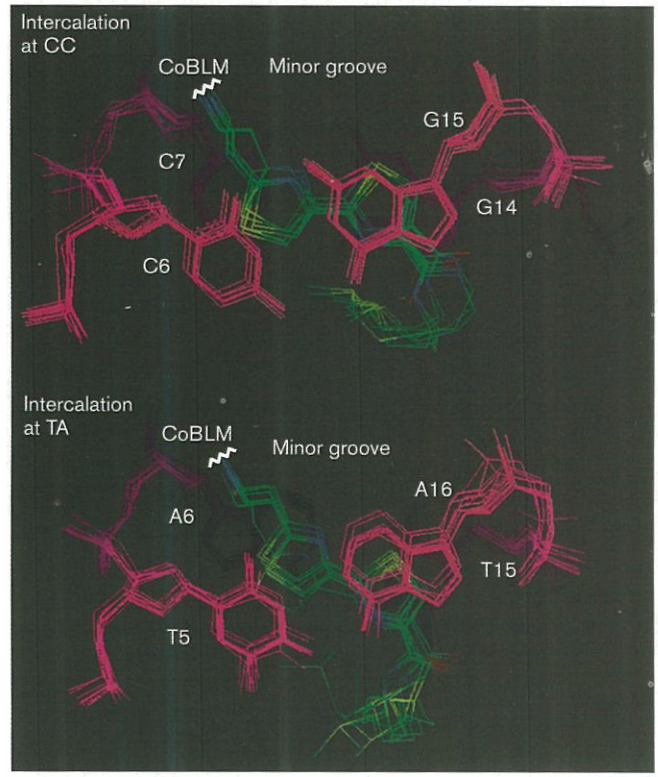

Comparison of the bithiazole stacking in the final averaged structures of the HOO-CoBLM complexes with **1** and **2**, from a view perpendicular to the plane of the bases. The stacking of the terminal thiazolium ring in **1** leads to substantially more overlap with the bases compared to that in **2**. The penultimate thiazolium ring is partially stacked between the bases in both complexes **1** and **2**.

orientation of the B-CH5 and B-C5H′ protons (Figure 6). As found previously for **1**, there are no obvious interactions between the bithiazole and the base pairs that suggest any sequence specificity. But the stacking of the thiazolium rings is, perhaps not unexpectedly, subtly different from that observed with **1**. The terminal thiazolium ring is not as well stacked between T15 and A16 as between G14 and G15 in the case of **1**. We will return to this point when discussing a reason why GTAC might be a hot spot for ds cleavage.

Consistent with our previous studies, our model suggests that the cleavage specificity of BLM is derived from the apparent hydrogen bonds (Figure 5) between the pyrimidine moiety (P in Figure 1) of HOO-CoBLM and the G4 on the 5′ side of the cleavage site. One of these interactions, which would be favorable for purines in general, is between one of the hydrogens of the 4-amino group of the pyrimidine ring and the N3 of G4 (distance = 1.92 ± 0.01 Å, angle = 174 ± 2°). A second possible hydrogen bond is between N3 of the pyrimidine ring on HOO-CoBLM and the non base-pairing hydrogen of the 2-amino of G4 (distance = 2.13 ± 0.05 Å, angle = 174 ± 1°), and confers a further preference for dG over dA on the 5′ side of the cleavage site. This hydrogen bond pattern between the G4•C17 base pair and the pyrimidine moiety of the drug is in essence a base triple (three bases are hydrogen bonded), but is distinct from previously observed base triples by its location in the minor groove. Finally, the primary amide proton of the propionamide of BLM is within hydrogen bonding distance to the O2 of C17 (distance = 1.92 Å ± 0.02, angle = 171 ± 4°), which might also contribute to the specificity.

Chemical specificity of cleavage

The detection of the hydroperoxide proton by NMR, and the multiple NOEs detected between this proton and **2** provided the constraints required to define its position relative to the site of hydrogen atom abstraction, 4′-H of T5. This proximity is manifested in the upfield chemical shift of T5-H4′ to 3.28 ppm (Tables 1,2; Figure 3), from 4.18 ppm in free DNA. As previously observed in the HOO-CoBLM complex with **1** and free in solution, the hydroperoxide appears to be stabilized by potential hydrogen bonding interactions of its penultimate oxygen with V-NH and T-NH of the linker region (V-NH to O distance is 1.85 ± 0.03 Å with an angle of 144 ± 5°; T-NH to O distance is 1.85 ± 0.07 Å with an angle of 153 ± 2°). As mentioned earlier, the hydrogen of the hydroperoxide is

also within hydrogen bonding distance to the carbonyl of the T (distance is 1.80 ± 0.02 Å with an angle of 147 ± 3°).

DNA conformation in the complex with HOO-CoBLM

The binding of HOO-CoBLM to **2** leads to several specific perturbations of the DNA structure that are consistent with what we observed with **1**. Previous studies of HOO-CoBLM with **1** have revealed that the sugar conformation of C6 undergoing hydrogen atom abstraction, is close to 3′-*endo* [28]. This sugar conformation deviated from the generic B-form conformation (2′-*endo*) of the other deoxynucleotides in **1**. A similar observation is made for the sugar conformation of T5 in **2**.

An unusual feature of the structure was apparent from the NOESY experiment in H_2O and is associated with the A3•T18 base pair, two base pairs removed from the cleavage site. The chemical shift of the A3 imino proton is shifted upfield in comparison to that in the free DNA and the imino proton of the A13•T8 base pair. In the structures generated from molecular dynamics calculations, significant deviations from B-form DNA are consistently observed at two base pairs 5′ to the cleavage site: (C2•G19)–(A3•T18) and (A3•T18)–(G4•C17). For instance, relative to what would be expected in a generic B-form base pair, the A3•T18 base pair is shifted towards the minor groove (by ~1.2 Å) and slides toward the strand containing A3 (by ~0.4 Å). The G4•C17 base pair, on the other hand, shifts (by ~1.4 Å) towards the major groove and slides (by ~0.4 Å) towards the strand containing C17. The net effect of this conformational change is that it places the A3•T18 imino proton directly under the G19 purine ring (Figure 7). The resulting shielding environment of this proton can account for the observed upfield chemical shift. Interestingly, the observation of a distortion of the DNA two base pairs 5′ removed from the cleavage site is consistent with the footprinting studies of Chang and Meares [32]. Studying the interaction of CoBLM and DNA with dimethylsulfate, they reported that binding of CoBLM significantly enhanced methylation of G1 relative to G2, 5′ to the cleavage site at T3 in the 5′G1–G2–T3 3′ sequence. They suggested that this enhanced methylation resulted from a conformational change associated with CoBLM binding. A conformational change, 5′ to the cleavage site, is also apparent from the ^{31}P studies (Table 1; Figure 3), where the G4pT5 phosphate directly 5′ to the intercalation site and the T15pA16 phosphate at the intercalation site are both shifted downfield relative to the other phosphate resonances. Although the basis for the long-range conformational change associated with HOO-CoBLM binding is unclear, this perturbation can account for the upfield shift of the A3•T18 imino proton and the previous biochemical studies of Chang and Meares [32].

Finally, one clear distinction between the HOO-CoBLM bound to **1** and **2** is apparent from examining the degree of

Figure 7

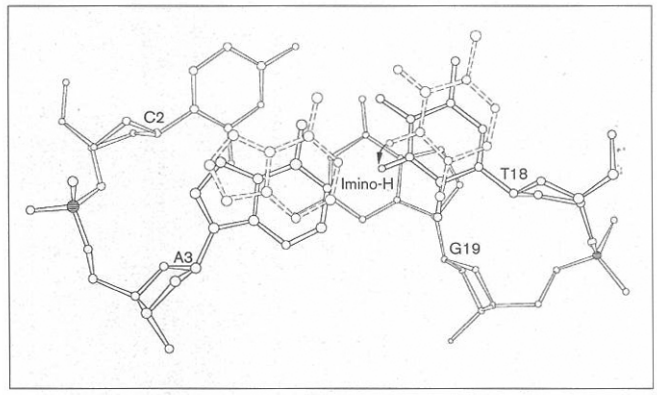

The position of the T18 imino proton over the G19 ring system in the complex, compared to its position in free DNA, as viewed from a position perpendicular to the plane of A3•T18 base pair. The C2•G19 (background) and A3•T18 (foreground) base pairs in the model of the complex are drawn as solid lines and atoms, and the position of the A3•T18 base pair in an ideal B form is illustrated with dashed bonds. The shift of the imino hydrogen from the uncomplexed to the complexed DNA is shown with an arrow.

stacking of the bithiazole of DNA with bases at its intercalation site (Figure 6). As indicated earlier, when bound to **2** neither ring of the bithiazole is fully stacked with the adjacent base pairs, in contrast to previous studies with **1** where the terminal thiazolium ring was completely stacked between G14 and G15 [28]. In addition, the complex of HOO-CoBLM with **2** is less well defined in the region of the bithiazole and the two base pairs on either side of the cleavage site, when compared to the complex with **1**. The family of molecular dynamics structures obtained for each of the two complexes were determined by approximately the same number of distance constraints, and satisfy their respective constraints equally well (Table 6; Table 5 in [28]). Nonetheless, the structures obtained for the complex with **2** are more diverse than those obtained for the complex with **1**, especially around the intercalation site. In the complex with **2**, the root mean square (rms) deviation from the mean structure of the 18 structures obtained by molecular dynamics simulations, found by comparison of the atoms of the bithiazole and the G4–T5–A6–C7 base pairs, was 0.64 ± 0.19 Å. The rms deviation in ten structures obtained by molecular dynamics calculations of HOO-CoBLM bound to **1**, for the bithiazole and the G5–C6–C7– T8 base pairs was 0.36 ± 0.09 Å. The higher rms deviation in the complex with **2** suggests that the interaction between the bithiazole and the d(TpA) motif observed in **2** is either not as stable as, and/or is more dynamic than the interaction with the d(CpC) motif observed in **1**. This difference might also explain the observation that the imino protons of T5 and T15 are not shifted upfield upon BLM binding, and that the chemical shift associated with the phosphate between the G4 and

T5 is shifted downfield, less than in the corresponding position of the complex of HOO-CoBLM with **1**. Considering the observed heterogeneity in the stacking patterns of nucleic acids in general [42], it is not surprising that the geometry of the intercalated bithiazole would be subject to some of the same subtle influences of the DNA sequence context. Although the hydrogen bonding between the pyrimidine moiety of HOO-CoBLM and a purine of DNA would be the primary determinant of sequence specific cleavage, the stability and kinetics of the intercalation of the bithiazole could be involved in the partitioning among all possible cleavage sites and between ss and ds cleavage events.

Implications for double-stranded DNA cleavage

The dynamic nature of the bithiazole moiety between the two A•T base pairs in **2** containing the hot spot for ds cleavage, might provide an explanation for how a single BLM molecule can catalyze cleavage at T5 and then reorganize to the opposite strand and catalyze cleavage at T15 without completely dissociating from the DNA. In an attempt to find the minimal structural reorganization required for ds cleavage, several models were constructed to mimic the translocation of the metal-binding domain of BLM from the first cleavage site to the second by simple rotation of HOO-CoBLM around given bonds.

As a starting point, the structure of HOO-CoBLM bound to **2** was first energy minimized without the distance constraints. HOO-CoBLM was then rotated ~180° around the (B-C4′)–(B-C2) bond (Figure 1). To remove steric clashes following the initial conformational change, and to position the metal-binding domain approximately in the minor groove of the second cleavage site, the bithiazole ring system was further rotated ~117° around an axis perpendicular to the plane of the bithiazole rings while keeping the ring system coplanar to DNA base pairs (Figure 8b,c). Finally, the structure was energy minimized to an rms gradient of 0.1. This reorganization resulted in a structure that could lead to hydrogen abstraction at T15•H4′. The structure allows for all the putative hydrogen bond interactions between the metal-binding region and the G14 on the 5′ side of the second cleavage site (T15) and positions the terminal oxygen of the hydroperoxide 3.2 Å from the 4′ hydrogen of T15 (Figure 8a). The penultimate thiazolium ring at the second cleavage site is now partially stacked between T15 and A16 (compare Figure 8b and 8c) in contrast to its stacking between T5 and C6 at the first cleavage site. The terminal thiazolium ring is partially stacked between T5 and A6 in contrast to its original position between T15 and A16 at the first cleavage site. In essence, the relative orientation of the two thiazolium rings with respect to the second cleavage site (T15) is the same as that observed at the first cleavage site (T5). Several other modeling attempts, including the rotation (by ~180°) of the (B-Cα)–(B-C2′) bond or the (T-Cα)–(T-CO) bond, were made to effect similar translocation of the metal-binding domain. In all cases, even more extensive modifications of the backbone torsion angles did not result in a model capable of hydrogen bonding with G14 or positioning the terminal oxygen of the hydroperoxide ligand closer than 4.1 Å to 4′ hydrogen of T15.

The feasibility of the *trans* to *cis* rotation of the bithiazole moiety in triggering the ds cleavage requires significant mobility of the penultimate thiazolium ring in the minor groove at the first cleavage site. This flexibility is likely to be facilitated by the relatively poor stacking observed between the bithiazole and two AT base pairs in **2**. In addition, the reorganization of the bithiazole is perhaps more appealing when considered in the context that DNA structural changes follow the first cleavage event. The strand scission is accompanied by the loss of three out of five carbons of the T5 deoxyribose as the base propenal and is likely to further disrupt the stacking of the penultimate thiazolium ring with T5, while keeping the intercalated terminal thiazolium ring relatively intact. It should be pointed out, however, that the timing of the complex DNA cleavage chemistry including strand scission relative to the kinetics of reorganization has not yet been established [18]. Although not intended to provide a definitive description of the process leading to the second cleavage event, the above modeling exercise suggests that the *trans* to *cis* rotation of the two thiazolium rings within the bithiazole moiety requires a relatively small conformational change to acquire a position that could result in ds cleavage.

Minor complex

The observation of a minor complex in the titration of **2** with HOO-CoBLM initially lead to the hypothesis that it might be associated with the cleavage at the secondary cleavage site T15 in the GTAC hot spot for DNA cleavage. Efforts were therefore made to assign some of the protons associated with this complex. The downfield shifted proton at 9.11 ppm (Figure 4 in [27]) can probably be assigned to the H-C2H. This proton exhibits NOEs to protons at 1.23 ppm and 0.60 ppm, probably associated with T-CH_3 and V-αCH_3, respectively. Unfortunately, no NOEs to DNA protons were detected and no additional protons could be assigned with certainty. Efforts to change the ratio of the major to minor complex by changing the temperature between 7–40°C, in an effort to increase the population of the minor species, were unsuccessful. The possibility that the minor complex is associated with a diastereomer of HOO-CoBLM [43,44] or the binding of HOO-CoBLM to a second site of **2** have been considered and discarded. The former is unlikely as there is no evidence for a diastereomeric mixture in the NMR spectrum of free HOO-CoBLM and the latter is unlikely as a fourfold excess of drug to DNA fails to reveal additional cleavage sites. Thus the identity of this second binding mode remains an intriguing mystery.

Figure 8

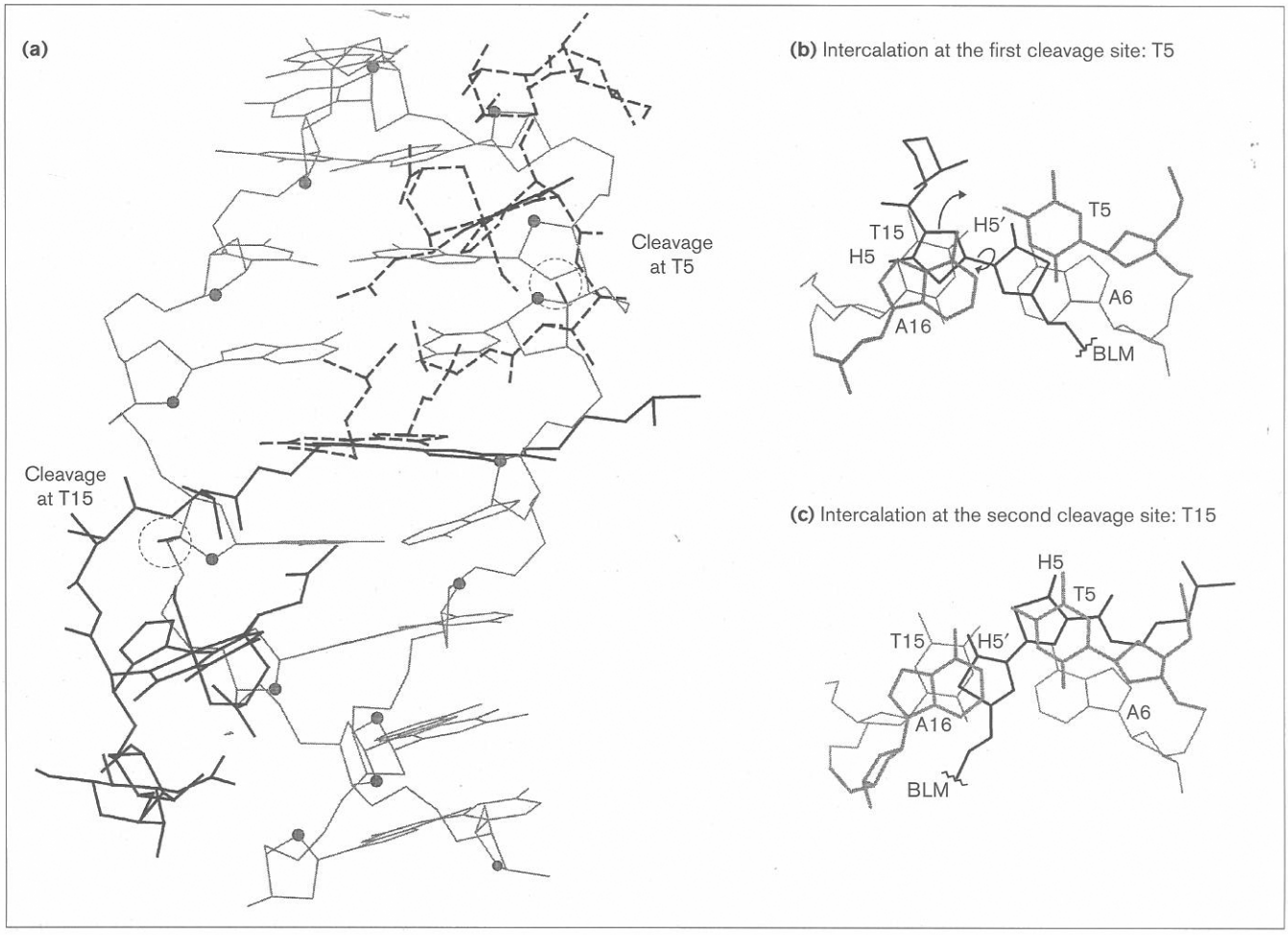

A comparison of the final averaged structure of HOO-CoBLM at the first cleavage site (T5) with the model of HOO-CoBLM at the second cleavage site (T15). **(a)** The translocation of the metal-binding domain of HOO-CoBLM from T5 (dashed lines) to T15 (solid lines) by a rotation around the (B-C4′)–(B-C2) bond and the repositioning of the bithiazole. The 4′ hydrogens at T5 and T15 are circled and the O4′ of DNA is shown as a gray sphere. **(b)** The *trans* orientation of the intercalated thiazolium rings at the first cleavage site. To reposition the metal-binding domain for the second cleavage event, a 180° rotation was made around the (B-C4′)–(B-C2) bond (see Figure 1) followed by a ~117° rotation of the bithiazole around an axis perpendicular to the bithiazole rings, which led to the stacking at the second cleavage site. **(c)** The *cis* orientation of the intercalated thiazolium rings at the second cleavage site. In both (b) and (c), the bithiazole and sulfonium moieties are shown in black and the DNA in gray. The T5•A16 base pair is in the foreground and the A6•T15 base pair in the background.

Significance

The studies of the interaction of the hydroperoxide form of cobalt bleomycin A2 (HOO-CoBLM) with d(CCAC*T*ACTGG) reveal that the binding mode and the basis for sequence recognition for d(GpT) motifs is similar to those for d(GpC) motifs. Nuclear magnetic resonance spectroscopy showed that the chemical shifts of the bithiazole protons in the complex with DNA are upfield shifted relative to those in free HOO-CoBLM. The specificity for guanines 5′ to the pyrimidine cleavage site is apparent from the unusual exchangeable proton that is associated with the 4-amino group of the pyrimidine of HOO-CoBLM, the chemical shift of which is downfield shifted to >10 ppm. Interestingly, a recent report of Mao *et al.* [24] on the binding of HOO-CoBLM to d(GGAAG*C*TTCC) and d(AAACG*T*TT) revealed similar upfield shifts for the bithiazole protons' chemical shifts and the presence of an exchangeable proton, in each case, at >10 ppm. While, no models of structures have appeared from this work so far, our data suggest that the model of Mao *et al.* will be very similar to ours. A comparison of their model structures with ours will eventually lead to a better understanding of the importance of the DNA binding and cleavage specificity of metallo-BLMs. Our preliminary modeling studies indicate that a simple *trans* to *cis* rotation of the first thiazolium ring relative to the second could be a trigger in relocating the metal-binding domain of BLM from the first cleavage site to the second.

Materials and methods

Sample preparation

The decameric oligonucleotide **2** was synthesized by the MIT biopolymer lab (MA, USA) and purified as previously described [27]. The purified DNA was desalted in a dialysis chamber against 50 mM sodium phosphate at pH 6.8. Its extinction coefficient was calculated to be $\varepsilon_{260} = 1 \times 10^5 M^{-1}cm^{-1}$. The HOO-CoBLM was prepared and purified as previously described [27].

NMR experiments

The NMR sample (2–3 mM complex in 50 mM sodium phosphate at pH 6.8) was prepared by titrating **2** with HOO-CoBLM and monitoring by NMR spectroscopy. For experiments in D_2O, the complex sample was lyophilized four times from 99.9% D_2O and then dissolved in 99.996% D_2O; for experiments in H_2O, the complex was dissolved in 90% H_2O/10% D_2O.

All NMR experiments were performed on either a 750 MHz Varian NMR spectrometer, or a 600 MHz or 500 MHz custom-built instrument at the Francis Bitter Magnet Laboratory. NMR data was processed using Felix (version 2.3, Molecular Simulations Inc., formally Biosym Technologies, Inc.) running on a Silicon Graphics work station. ^1H and ^{13}C chemical shifts were referenced to an internal standard, sodium 3-(trimethylsilyl)-1-propanesulfonate at 0.00 ppm. ^{31}P chemical shifts were referenced to an external sample of trimethyl phosphate, which is 3.53 ppm downfield of 85% H_3PO_4.

DQF-COSY, TOCSY (using Z-filtered TOWNY or DIPSI-2 isotropic mixing sequence with 35 ms, 70 ms, and 140 ms mixing times) [45–47] and NOESY (100 ms, 200 ms, and 400 ms mixing times) experiments were recorded at 20°C in D_2O and/or H_2O. For experiments in D_2O, data sets with 4096×512 complex points were acquired with sweep widths of 5500 Hz (500 MHz instrument) or 8000 Hz (750 MHz instrument) in both dimensions and 32 scans per t_1 increment. During the relaxation delay period, a 2.0 s presaturation pulse was used for solvent suppression. For the NOESY experiments in H_2O, a Watergate pulse sequence [48] was used, and data sets with 4096×512 complex points were acquired with sweep widths of 12,000 Hz (750 MHz instrument) in both dimensions. The t_1 dimension was zero-filled to 4096 data points and spectra were processed with a combination of exponential and Gaussian weighting functions. In all cases, ridges in t_1 were reduced by multiplying the first point in t_1 by one half prior to the Fourier transform. Baselines were corrected with an automatic baseline correction routine in t_2 when necessary.

HMQC spectra were recorded at 20°C in D_2O with a J_{C-H} coupling constant of 165 Hz. Data sets with 2048×256 complex points were acquired with 6000 Hz (^1H) and 25,000 Hz (^{13}C) sweep widths on a 500 MHz instrument. 128 scans were collected for every t_1 increment. During the relaxation delay period, a 1.5 s presaturation pulse was used for solvent suppression. The t_1 dimension was zero-filled to 2048 data points. Spectra were then processed with an exponential weighting function.

An indirect detected ^{31}P–^1H COSY experiment [49] in D_2O was recorded at 20°C on a 600 MHz instrument. Data sets with 4096×256 complex points were acquired with 7000 Hz in the ^1H dimension and 2000 Hz in the ^{31}P dimension.

Molecular modeling

All calculations were carried out with CHARMm 24 [50] on a Cray Y-MP or J-90. The structural calculations were set up as described previously [27,28], with the following exceptions. The calculation of non-bonded van der Waals and electrostatic interactions were truncated at 13 Å, using a force switching function between 8 Å and 12 Å. The list of non-bonded terms was updated every 20 steps, except in the final molecular dynamics (MD) run, where the list was updated if an atom moved >0.5 Å. The terms for electrostatic interactions and hydrogen bonds were only included in the final 15 ps step of the calculation. Following heating, the temperature was maintained by scaling the velocities of the atoms as necessary to keep the temperature at 300±10K. In the final 15 ps MD phase, scaling was only required 1–2 times. Because the treatment of non-bonded interactions just described is slightly different than the conditions used to model the complex of HOO-CoBLM with **1** [28], the structural calculations for HOO-CoBLM with **1** were repeated using the current conditions so the complexes with d(GpC) and d(GpT) sequences could be compared directly. There were no significant differences from the structure with **1** as previously reported except where noted in the Results and discussion section.

Bleomycin A2 was constructed as previously described [27], with the exception that the bond lengths and bond angles of the thiazolium rings were based on the X-ray crystal structures of bithiazole analogs [51,52]. The DNA was constructed in Quanta in either an A-form or B-form conformation. The charges on the non-bridging oxygens of the phosphate groups were reduced to lower the overall charge on phosphate to −0.32 [53]. The program CURVES [54,55] was used to measure DNA conformational parameters. To allow for potential distortion of the DNA as a result of the intercalation of the bithiazole moiety, lower force constants were used on the base pairs of the intercalation site, and those directly adjacent to it. The δ and χ angles were not constrained. The dihedral angle constraints with a force constant of 30 kcal mol^{-1} Å^{-2} rad^{-2} were used throughout the molecular dynamics simulations on DNA base pairs to prevent excessive propeller twist and buckling. These constraints were not applied at the intercalation site (T5•A16 and A6•T15). The intramolecular distance constraints used for DNA included restraints to maintain Watson–Crick hydrogen bonding. No other distance constraints were used in any modeling procedure that were not derived from an observed NOESY crosspeak.

Distance constraints

There were a total of 59 intermolecular NOEs (Table 4), 75 intramolecular CoBLM NOEs (Table 5), 223 intramolecular DNA NOEs, and 26 Watson–Crick hydrogen bond constraints. These NOEs were classified as strong, medium, or weak based on visual inspection of the crosspeak intensities in the 200 ms NOESY spectra. The distance constraints were set at 1.9–3.0 Å, 1.9–4.0 Å, and 3.0–5.0 Å for strong, medium, and weak NOEs, respectively. An additional 1 Å was added to the upper limit of constraints for the methyl or methylene hydrogen pseudoatoms. DNA intramolecular constraints were set at 1.9–3.0 Å, 2.5–4.0 Å, and 3.5–5.0 Å for strong, medium, and weak NOEs, respectively.

Dihedral angle constraints

The analysis of the coupling constants in HOO-CoBLM of the complex was based on visual inspection of the crosspeak sizes in the DQF-COSY spectra collected in D_2O and H_2O. A *trans* orientation of the protons was defined by a large coupling constant (>8 Hz), while a *gauche* conformation was defined by a small coupling constant (<4 Hz).

Initial structure

The initial structure was constructed by manually docking the bithiazole moiety between T5•A16 and A6•T15 in a B-form model of **2**. The position of the bithiazole was determined by the intermolecular NOEs observed between the bithiazole and the DNA, which are consistent with only the *trans* orientation of the thiazolium protons (Table 4). Using the backbone dihedral angles of the bithiazole, threonine, and valeryl moieties (B, T and V in Figure 1), the position of the metal binding region was adjusted to relieve unfavorable van der Waals contacts between the metal binding region and the minor groove. After this crude positioning, this preliminary structure was minimized by 200 steps of the steepest descent method, followed by conjugate gradient minimization to a rms gradient <0.1, and finally by the conjugate gradient method using the dihedral and distance constraints, to a rms gradient <0.1.

Molecular dynamics simulations

The structures that satisfied the experimental constraints were generated using 20 calculations of restrained molecular dynamics simulated

annealing, following the protocol described previously [27,28]. The protocol consisted of heating the system to 1000K with weak distance constraints (6ps) , gradually increasing the force constants applied to the distance constraints (6.5ps), a high temperature equilibration (10ps), slow cooling to 300K (7ps), gradual introduction of the dihedral constraints (10ps), and a final molecular dynamics stage (15ps). The final structure for each iteration was generated by averaging the coordinates of the final 5ps of the 15ps molecular dynamics simulation, followed by 2000 steps of conjugate gradient minimization with the distance constraints and HOO-CoBLM dihedral angle constraints. The DNA backbone constraints were not used in the minimization. In early stages of refinement, the average structures generated from the initial A-form or B-form DNA were found to differ from one another by ~0.5Å. Based on these similarities, the final simulated annealing calculations used the B-form model as a starting structure.

Acknowledgements

This research is supported by NIH grant GM 34454 to J.S. The NMR facility is supported by NIH grant P41RR0095. We are grateful to J. Williamson for many helpful discussions.

References

1. Umezawa, H., Maeda, K., Takeuchi, T. & Okami, Y. (1966). New antibiotics, Bleomycin A and B. *J. Antibiot.* **19**, 200–209.
2. Lazo, J.S., Sebi, S.M. & Schellens, J.H. (1996). Bleomycin. *Cancer Chemother. Biol. Response Modif.* **16**, 39–47.
3. Mir, L.M., Tounekti, O. & Orlowski, S. (1996). Bleomycin: revival of an old drug. *Gen. Pharmacol.* **27**, 745–748.
4. Hecht, S.M., ed. (1979). Bleomycin: chemical, biochemical, and biological aspects, Springer-Verlag, New York, USA.
5. Stubbe, J. & Kozarich, J.W. (1987). Mechanisms of bleomycin-induced DNA degradation. *Chem. Rev.* **87**, 1107–1136.
6. Petering, D.H., Byrnes, R.W. & Antholine, W.E. (1990). The role of redox-active metals in the mechanism of action of bleomycin. *Chem. Biol. Interactions* **73**, 133–182.
7. Povirk, L.F. & Austin, M.J.F. (1991). Genotoxicity of Bleomycin. *Mut. Res.* **257**, 127–143.
8. Magliozzo, R.S., Peisach, J. & Ciriolo, M.R. (1989). Transfer RNA in cleaved by activated bleomycin. *Mol. Pharmacol.* **35**, 428–432.
9. Hecht, S.M. (1994). RNA degradation by bleomycin, a naturally occurring bioconjugate. *Bioconj. Chem.* **5**, 513–526.
10. Kane, S.A. & Hecht, S.M. (1994). Polynucleotide recognition and degradation by bleomycin. In *Polynucleotide Recognition and Degradation by Bleomycin* (Cohn, W.E. & Moldave, K., eds), pp 313–352, Academic Press, San Diego, USA.
11. Sausville, E.A., Peisach, J. & Horwitz, S.B. (1976). A role for ferrous ion and oxygen in the degradation of DNA by Bleomycin. *Biochem. Biophys. Res. Commun.* **73**, 814–822.
12. Sausville, E.A., Peisach, J. & Horwitz, S.B. (1978). Effect of chelating agents and metal ions on the degradation of DNA by Bleomycin. *Biochemistry* **17**, 2740–2746.
13. Sam, J.W., Tang, X.-J. & Peisach, J. (1994). Electrospray mass spectrometry of iron-bleomycin: demonstration that activated bleomycin is a ferric peroxide complex. *J. Am. Chem. Soc.* **116**, 5250–5256.
14. Giloni, L., Takeshita, M., Johnson, F., Iden, C. & Grollman, A.P. (1981). Bleomycin-induced strand-scission of DNA. *J. Biol. Chem.* **256**, 8608–8615.
15. Rabow, L.E., McGall, G.H., Stubbe, J. & Kozarich, J.W. (1990). Identification of the source of oxygen in the alkaline-labile product accompanying cytosine release during bleomycin-mediated oxidative degradation of d(CGCGCG). *J. Am. Chem. Soc.* **112**, 3203–3208.
16. Rabow, L.E., Stubbe, J. & Kozarich, J.W. (1990). Identification and quantitation of the lesion accompanying base release in bleomycin-mediated DNA degradation. *J. Am. Chem. Soc.* **112**, 3196–3203.
17. Hecht, S.M. (1986). The chemistry of activated BLM. *Acc. Chem. Res.* **19**, 383–391.
18. Burger, R.M., Drlica, K. & Birdsall, B. (1994). The DNA cleavage pathway of iron bleomycin. *J. Biol. Chem.* **269**, 25978–25985.
19. Povirk, L.F., Han, Y.-H. & Steighner, R.J. (1989). Structure of bleomycin-induced DNA double-strand breaks: predominance of blunt ends and single-base 5′ extensions. *Biochemistry* **28**, 5808–5814.
20. Steighner, R.J. & Povirk, L.F. (1990). Bleomycin-induced DNA lesions at mutational hot spots: implications for the mechanism of double-strand cleavage. *Proc. Natl Acad. Sci. USA* **87**, 8350–8354.
21. Absalon, M.J., Stubbe, J. & Kozarich, J.W. (1995). Sequence-specific double-strand cleavage of DNA by Fe-Bleomycin. 1. The detection of sequence-specific double-strand breaks using hairpin oligonucleotides. *Biochemistry* **34**, 2065–2075.
22. Absalon, M.J., Wu, W., Stubbe, J. & Kozarich, J.W. (1995). Sequence-specific double-strand cleavage of DNA by Fe-bleomycin. 2. mechanism and dynamics. *Biochemistry* **34**, 2076–2086.
23. Stubbe, J., Kozarich, J.W., Wu, W. & Vanderwall, D.E. (1996). Bleomycins: a structural model for specificity, binding, and double strand cleavage. *Acc. Chem. Res.* **29**, 322–330.
24. Mao, Q., Fulmer, P., Li, W., DeRose, E.F. & Petering, D.H. (1996). Different conformations and site selectivity of HO_2--Co(II)-bleomycin A2 and Co(III)-bleomycin A2 bound to DNA oligomers. *J. Biol. Chem.* **271**, 6185–6191.
25. Manderville, R.A., Ellena, J.F. & Hecht, S.M. (1995). Interaction of Zn(II)Bleomycin with $d(CGCTAGCG)_2$. A binding model based on NMR experiments and restrained molecular dynamics calculations. *J. Am. Chem. Soc.* **117**, 7891–7903.
26. Wu, W., Vanderwall, D.E., Stubbe, J., Kozarich, J.W. & Turner, C.J. (1994). Intercalation of Co bleomycin A2 (green) with $d(CCAGGCCTGG)_2$: evidence for intercalation using 2D NMR. *J. Am. Chem. Soc.* **116**, 10843–10844.
27. Wu, W., Vanderwall, D.E., Lui, S.M., Tang, X.-J., Turner, C.J., Kozarich, J.W. & Stubbe, J. (1996). Studies of Co Bleomycin A2 green: its detailed structural characterization by NMR and molecular modeling and its sequence-specific interaction with DNA oligonucleotides. *J. Am. Chem. Soc.* **118**, 1268–1280.
28. Wu, W., Vanderwall, D.E., Turner, C.J., Kozarich, J.W. & Stubbe, J. (1996). Solution structure of Co Bleomycin A2 green complexed with d(CCAGGCCTGG). *J. Am. Chem. Soc.* **118**, 1281–1294.
29. Boger, D.L., Colletti, S.L., Teramoto, S., Ramsey, T.M. & Zhou, J. (1995). Synthesis of key analogs of Bleomycin A2 that permit a systematic evaluation of the linker region: identification of an exceptionally prominent role for the L-threonine substituent. *Bioorg. Med. Chem.* **3**, 1281–1295.
30. Boger, D.L., Teramoto, S., Honda, T. & Zhou, J. (1995). Synthesis and evaluation of the fully functionalized bleomycin A2 metal binding domain containing the 2-O-(3-O-carbamoyl-α-D-mannopyranosyl)-α-L-gulopyranosyl disaccharide. *J. Am. Chem. Soc.* **117**, 7338–7343.
31. Boger, D.L., Teramoto, S. & Zhou, J. (1995). Key synthetic analogs of bleomycin A2 that directly address the effect and role of the disaccharide: demannosylbleomycin A2 and α-D-mannopyranosyl-deglycobleomycin A2. *J. Am. Chem. Soc.* **117**, 7344–7356.
32. Chang, C.-H. & Meares, C.F. (1984). Cobalt-bleomycins and deoxyribonucleic acid: sequence-dependent interactions, action spectrum for nicking, and indifference to oxygen. *Biochemistry* **23**, 2268–2274.
33. Saito, I., Morii, T., Sugiyama, H., Matsura, T., Meares, C.F. & Hecht, S.M. (1989). Photoinduced DNA strand scission by cobalt bleomycin green complex. *J. Am. Chem. Soc.* **111**, 2307–2308.
34. Worth L. Jr., Frank, B.L., Christner, D.F., Absalon, M.J., Stubbe, J. & Kozarich, J.W. (1993). Isotope effects on the cleavage of DNA by bleomycin: mechanism and modulation. *Biochemistry* **32**, 2601–2609.
35. Wüthrich, K. (1986). NMR of proteins and nucleic acids, John Wiley & Sons, Inc, New York, USA.
36. Gao, X. & Patel, D.J. (1989). Antitumor drug-DNA interaction: NMR studies of echinomycin and chromomycin complexes. *Q. Rev. Biophys.* **22**, 93–138.
37. Addess, K.J., Gilbert, D.E., Olsen, R.K. & Feigon, J. (1992). Proton NMR studies [N-MeCys^3, N-MeCys^7] tandem binding to DNA oligonucleotides: sequence-specific binding at the TpA site. *Biochemistry* **31**, 339–350.
38. Gorenstein, D.G. (1992). ^{31}P NMR of DNA. *Methods Enzymol.* **211**, 254–286.
39. Xu, R.X., Nettesheim, D., Otvos, J.D. & Petering, D.H. (1994). NMR determination of the structures of peroxycobalt(III) bleomycin and cobalt(III) bleomycin, products of the aerobic oxidation of cobalt(II) bleomycin by dioxygen. *Biochemistry* **33**, 907–916.
40. Akkerman, M.A.J., Haasnoot, C.A.G. & Hilbers, C.W. (1988). Studies of the solution structure of the bleomycin-A2-zinc complex by means of two-dimensional NMR spectroscopy and distance geometry calculations. *Eur. J. Biochem.* **173**, 211–225.
41. Akkerman, M.A.J., Neijman, E.W.J.F., Wijmenga, S.S., Hilbers, C.W. & Bermel, W. (1990). Studies of the solution structure of the bleomycin A2-iron(II)-carbon monoxide complex by means of two dimensional NMR spectroscopy and distance geometry calculations. *J. Am. Chem. Soc.* **112**, 7462–7474.

42. Dickerson, R.E. (1986). DNA-drug binding and control of genetic information. In *DNA-Drug Binding and Control of Genetic Information* (Smi, M.G. & Grossman, L., eds), pp 245–255, Plenum, New York, USA.
43. Farinas, E.T., Tan, J.D. & Mascharak, P.K. (1996). Photoinduced DNA cleavage reactions by designed analogues of Co(III)-Bleomycin: the metalated core is primary determinant of sequence specificity. *Inorg. Chem.* **35**, 2637–2643.
44. Tan, J.D., Farinas, E.T., David, S. & Marscharak, P.M. (1994). NMR evidence of sequence specific DNA binding by a cobalt(III)-bleomycin analogue with tethered acridine. *Inorg. Chem.* **33**, 4295–4308.
45. Kadkhodaei, M.K., Hwang, T.-L., Tang, J. & Shaka, A.J. (1993). A simple windowless mixing sequence to suppress cross relaxation in TOCSY experiments. *J. Magn. Res. Ser. A* **105**, 104–107.
46. Rance, M. (1987). Improved techniques for homonuclear rotating-frame and isotopic mixing experiments. *J. Mag. Res.* **74**, 557–564.
47. Shaka, A.J., Lee, C.J. & Pines, A. (1988). Iterative schemes for bilinear operators; application to spin decoupling. *J. Mag. Res.* **77**, 274–293.
48. Sklenar, V., Piotto, M., Leppik, R. & Saudek, V. (1993). Gradient-tailored water suppression for ^{1}H-15N HSQC experiments optimized to retain full sensitivity. *J. Magn. Res. Ser. A* **102**, 241–245.
49. Sklenar, V., Miyashiro, H., Zon, G., Miles, H.T. & Bax, A. (1986). Assignment of the ^{31}P and ^{1}H resonance in oligonucleotides by two-dimensional NMR spectroscopy. *FEBS Lett.* **208**, 94–98.
50. Brooks, B.R., Bruccoleri, R.E., Olafson, B.D., States, D.J., Swaminathan, S. & Karplus, M. (1983). Chemistry at HARvard molecular modeling. *J. Comp. Chem.* **4**, 187–217.
51. Kuroda, R., Neidle, S., Riordan, J.M. & Sakai, T.T. (1982). X-ray crystallographic analysis of 3-(2′-phenyl-2,4′-bithiazole-4-carboxamido)propyldimethylsulphonium iodide, an analogue of the DNA-bonding portion of bleomycin A2. *Nucleic Acids Res.* **10**, 4753–4763.
52. Koyama, G., Hikaru, N., Yasuhiko, M., Takita, T., Maeda, K. & Umezawa, H. (1968). The chemistry of bleomycin. II. The molecular and crystal structure of a sulfur-containing chromophoric amino acid. *Tetrahed. Lett.* **44**, 4635–4638.
53. Manning, G.S. (1978). The molecular theory of polyelectrolyte solutions with applications to the electrostatic properties of nucleotides. *Q. Rev. Biophys. II*, **11**, 179–246.
54. Lavery, R. & Sklenar, H. (1988). The definition of generalized helicoid parameters and of axis curvature for irregular nucleic acids. *J. Biomol. Struct. Dynam.* **6**, 63–91.
55. Lavery, R. & Sklenar, H. (1989). Defining the structure of irregular nucleic acids. *J. Biomol. Struct. Dynam.* **6**, 655–667.